Modeling the Effects of Transcranial Magnetic Stimulation on Spatial Attention

Ying Jing[1], Ole Numssen[2], Konstantin Weise[1,3], Benjamin Kalloch[1,4], Jens Haueisen[4], Gesa Hartwigsen[2,5*], Thomas R. Knösche[1,4*]

1. Methods and Development Group Brain Networks, Max Planck Institute for Human Cognitive and Brain Sciences, Stephanstraße 1a, 04103, Leipzig, Germany.

2. Lise Meitner Research Group Cognition and Plasticity, Max Planck Institute for Human Cognitive and Brain Sciences, Stephanstraße 1a, 04103, Leipzig, Germany.

3. Advanced Electromagnetics Group, Technische Universität Ilmenau, Helmholtzplatz 2, 98693, Ilmenau, Germany.

4. Institute of Biomedical Engineering and Informatics, Technische Universität Ilmenau, Gustav-Kirchhoff-Straße 2, 98693, Ilmenau, Germany.

5. Wilhelm Wundt Institute for Psychology, Leipzig University, Neumarkt 9-19, 04109, Leipzig, Germany

Abstract

Transcranial magnetic stimulation (TMS) has been widely used to modulate brain activity in healthy and diseased brains, but the underlying mechanisms remain unclear. Previous research leveraged biophysical modeling of the induced electric field (E-field) to map causal structure-function relationships in the primary motor cortex. This study aims at transferring this localization approach to spatial attention, which helps to understand the TMS effects on a higher cognitive function, and may ultimately result in an optimized stimulation scheme. Thirty right-handed healthy participants participated in a functional magnetic imaging (fMRI) experiment and seventeen of them were re-invited for a TMS experiment. The fMRI activation peak within the right inferior parietal lobule (rIPL) during a Posner-like attention task defined the center target for TMS. Thereafter, participants underwent 500 Posner-task trials with 5 TMS pulses at 10 Hz each to modulate attentional processing. The TMS-induced electrical fields (E-fields) for every cortical target were correlated with the behavioral modulation to identify the relevant cortical regions for attentional orientation and reorientation. We found that TMS selectively inhibited attentional reorienting, resulting in task-specific behavioral impairments, and this effect was especially pronounced for stimulating the supramarginal gyrus (SMG). The BOLD-measured neuronal activity and TMS-evoked neuronal effects showed different patterns, which highlights the principal distinction between neural activity being correlated with (or maybe even caused by) particular paradigms, and activity of neural populations exercising a causal influence on the behavioral outcome.

Keywords

Transcranial magnetic stimulation, Electrical field, Brain mapping, Magnetic resonance imaging, Posner task, Attention

1. Introduction

Transcranial magnetic stimulation (TMS) is a non-invasive brain stimulation technique that allows the modulation of cortical function in vivo. It has been widely used to map structure-function relationships in healthy brains (Bestmann and Feredoes, 2013, Groppa et al., 2013), as well as for therapeutic application (Perera et al., 2016, Rawji et al., 2020). In brief, TMS induces an electric field (E-field) in the brain, which can temporarily excite or inhibit the stimulated area by depolarizing or hyperpolarizing cell membranes (Hallett, 2000). However, the precise location of the neuronal populations which are affected by the induced E-field and cause the observed behavioral or physiological changes are difficult to determine. Consequently, TMS studies show considerable interindividual variability in the observed outcome, which hampers its general efficacy in basic and clinical applications (Hartwigsen and Silvanto, 2022). The observed variability in TMS effects may be attributed to a complex interplay of interindividual differences (e.g., tissue resistivity, gyral shape, E-field direction, and magnitude) and the variable response of neuronal networks (Hartwigsen and Silvanto, 2022).

To address this issue, biophysical modeling of the induced E-field based on individual head anatomy has been increasingly used to estimate cortical locations and stimulation strengths at target areas (Van Hoornweder et al., 2022, Nieminen et al., 2015, Thielscher et al., 2015). Based on the biophysical properties of the head models, as well as the stimulation parameters such as intensity, location, and orientation of the TMS coil, the finite element method (FEM) provides realistic estimates of the induced E-field. By correlating the E-field with behavioral or physiological outcome measures, one may identify the neural structures that are effectively stimulated and underlie these effects (Bungert et al., 2017, Laakso et al., 2018, Hartwigsen et al., 2015). In this context, we recently established a novel method to localize the origin of the motor evoked potential (MEP) by combining measurements of hand muscle responses at different coil positions and orientations with simulations of the induced E-field (Numssen et al., 2021b, Weise et al., 2022, Weise et al., 2020). In this so-called “regression approach”, a non-linear (sigmoid-like) correlation between the local E-field and MEP is found at the cortical muscle representation within M1. So far, this powerful

modeling framework has exclusively been used in the primary motor cortex. The current study aims at exploring whether and how this approach may be transferred to the cognitive domain in the healthy human brain. We chose attention as a prototypical function which is relevant to all higher cognitive processes and plays a central role in everyday behavior (Johnson and Proctor, 2004, Schuwerk et al., 2017).

With respect to the underlying neural correlates of attention, it has been demonstrated that different subprocesses of attention are organized in various large-scale networks in the human brain (Corbetta and Shulman, 2002). In particular, two separate networks were identified for visuo-spatial attention, related to the voluntary deployment of attention (i.e., attentional orientation) and the reorientation to unexpected events (i.e., attentional reorientation), respectively (Vossel et al., 2014). Attentional orientation is associated with the dorsal attention network (DAN), which comprises the superior parietal lobule (SPL)/intraparietal sulcus (IPS) and the frontal eye fields (FEF) (Szczepanski et al., 2013). In contrast, the ventral attention network (VAN), including the right inferior parietal lobule (rIPL) and the ventral frontal cortex (VFC), is typically involved in detecting unattended stimuli and triggering attentional reorientation (Corbetta et al., 2008). Previous neuroimaging studies have identified the rIPL as a key region for attentional reorientation, and damage to this area can cause severe attention deficits (Igelström and Graziano, 2017, Numssen et al., 2021a). In this study, we applied TMS to the rIPL while participants were performing a Posner-like attentional task (Posner, 1980). We reasoned that direct modulation of task performance should provide insights into the underlying causal relevance of specific brain regions for a given task (Walsh and Cowey, 2000).

In summary, we first localized attentional processes with functional neuroimaging at the individual subject level and then applied TMS during the attention task over the individually identified rIPL region. Provided that stimulation of well-localized neural populations would be responsible for observed behavioral effects, correlating the individual E-field strength with those effects (i.e., modulations of reaction times) should identify the areas that are effectively stimulated.

Based on previous TMS studies in the domain of attention (Rushworth et al., 2001, Chambers et al., 2004), our main hypothesis was that interfering with rIPL activity during task performance should selectively modulate behavior during attentional reorientation without affecting attentional orientation. We focused on reaction time (RT) modulation to quantify causal effects of the TMS-induced E-fields on attentional processes in a continuous manner. The combination of a behavioral experiment with our previously established localization method should provide new insight into the

cortical areas that are relevant for attentional processing. A better understanding of the stimulation effects on cognitive functions will guide more effective stimulation protocols for research and clinical purposes.

2. Material and methods

We performed a functional magnetic resonance imaging (fMRI) and a TMS experiment to localize the neuronal populations that are responsible for the TMS effect (Figure 1). In the fMRI experiment, we calculated individual activation maps while participants performed the Posner-like task. In the subsequent TMS localization experiment, 500 TMS trials were performed, while the coil was placed at varying positions near the identified activation peak. The regression approach was performed to identify effective targets for attentional reorientation. Cortical locations with the highest correlation between the induced E-field and the behavioral consequences are assumed to be the optimal target for the perturbation of attentional function.

2.1. Participants

Thirty healthy volunteers (15 female, mean age 30.80 ± 5.31 years) were recruited for the fMRI experiment. All participants had normal or corrected to normal vision, and no psychiatric or neurological disorders, or contraindications against TMS or MRI. All participants were right-handed, with a mean laterality index of 90.77 (standard deviation, SD = 10.06) according to the Edinburgh Handedness Inventory (Oldfield, 1971). Written informed consent was obtained from each participant prior to the experiment. The study was approved by the local ethics committee of Leipzig University (ethics number: 371/19-ek). We re-invited seventeen participants (8 female, age 30.12 ± 5.84 years, laterality index 91.24 ± 9.46) to participate in the TMS experiment.

2.2. Behavioral task

We used an adapted version of Posner's location-cueing task (Rushworth et al., 2001, Numssen et al., 2021a, Thiel et al., 2004) to trigger orienting and reorienting of spatial attention. The fMRI version of the task contained three trial types: *valid*, *invalid*, and *neutral*, to target different attentional processes (Figure 1). The contrast between invalid and valid trials isolates attentional reorienting processes, and the contrast between valid and neutral trials defines attentional orienting processes/attentional benefits (Grosbras and Paus, 2002, Peelen et al., 2004). During the task, each trial started with the presentation of two rectangular boxes (each size 2.6° of visual angle,

with the center situated 8.3° left or right, positioned horizontally) and a fixation cross (size 0.88°) at the center of the screen. To avoid expectancy effects, the duration of fixation (interstimulus interval, ISI) was randomly set to either 2, 3, 4, or 5 s. Subsequently, an arrow was displayed for 250 or 350 ms which served as a cue for the upcoming target location. For valid cues (60 %), the arrow pointed at the side where the target appeared. Participants were trained to orient their attention towards the indicated target position while keeping their fixation at the central fixation cross. For invalid cues (20 %), the arrow pointed to the opposite side of the target, which required participants to reorient their attention to the target side. Neutral cues (20 %) did not contain any information about the target's location. Finally, a target was presented either at the left or right side (equally distributed) for 2 s. Participants were instructed to identify the targets' positions by pressing the right/left button using their index and middle fingers as fast and accurately as possible.

We included a total number of 250 trials in the fMRI experiment and 500 in the TMS experiment. The fMRI scan lasted 25 minutes with 150 valid trials, 50 invalid trials, and 50 neutral trials. Participants had a 30 s break in the middle of the task to prevent fatigue (Figure 1a). Before the MRI experiment, participants performed 10 trials as training outside the scanner. In the TMS experiment we specifically focussed on attentional reorienting and, thus, only presented valid (75 %) and invalid (25 %) trial types. The ISI was shortened to 3-4s (Figure 1b). The stimulation lasted approximately 60 min with a short break after every 100 trials. The order of trial types was randomized across participants. Stimuli were administered with Presentation software (v20.1, Neurobehavioral Systems, Berkeley, CA).

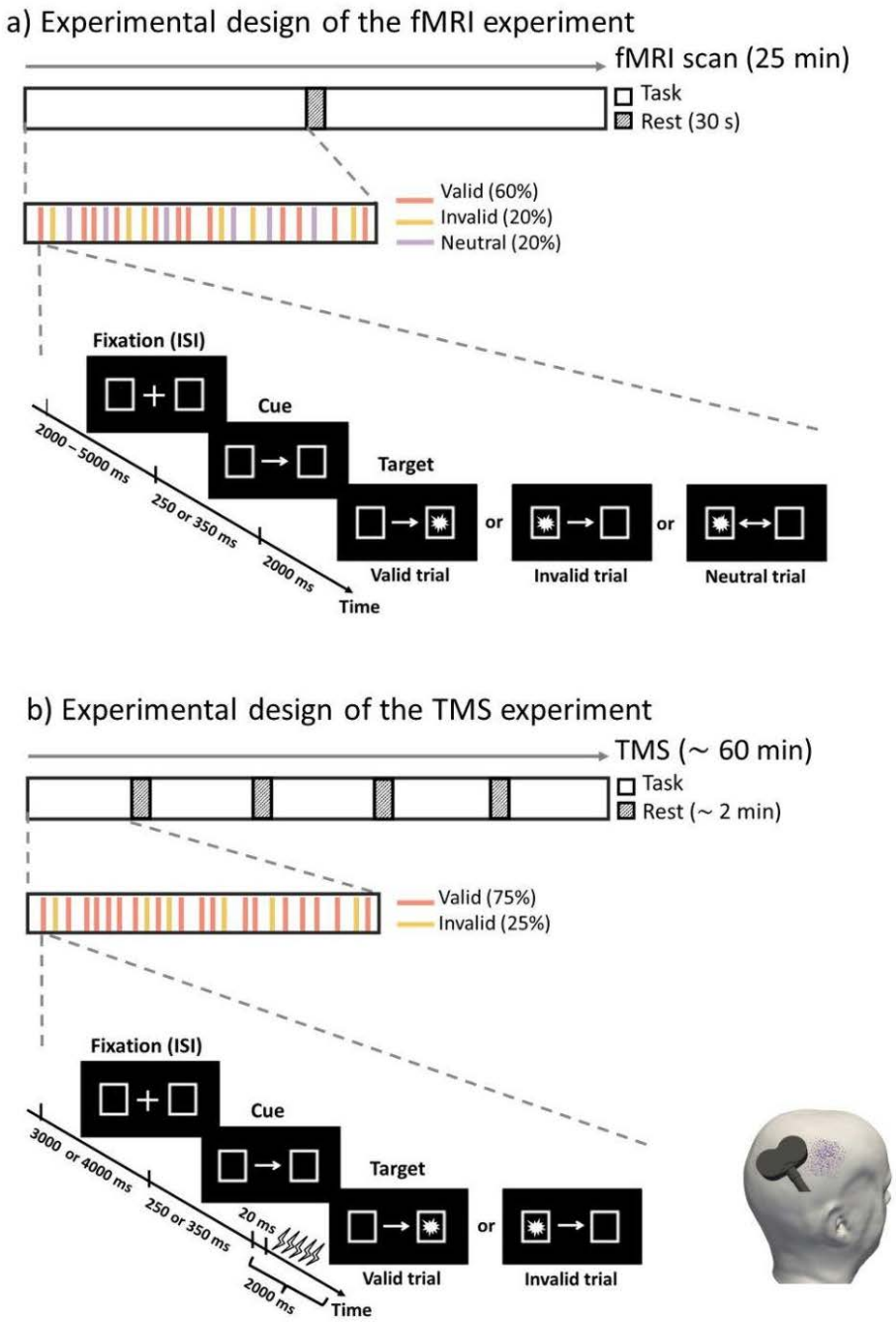

Figure 1. Task paradigm and experimental procedures for the fMRI (a) and TMS experiment (b). A trial consisted of a fixation phase (2-5 s in the fMRI experiment and 3-4 s in the TMS experiment), a cue phase (250 or 350 ms), and a target phase (2 s). Three types of trials (valid, invalid, and neutral) were included in the fMRI experiment, while the neutral condition was excluded in the TMS experiment. A total number of 250 trials were collected in the fMRI experiment. During the TMS experiment, a 5-pulse burst of 10 Hz rTMS was applied 20 ms after the presentation of the target for each trial. 500 TMS trials with random coil positions (represented by violet dots on the head model) and orientations were collected for further analysis.

2.3. MRI data acquisition

Both functional and structural MRI data were collected using a 3 Tesla Siemens Skyra fit scanner with a 32-channel head coil. To segment the main tissues of the head (scalp, skull, gray matter (GM), white matter (WM), cerebrospinal fluid (CSF), and ventricle) for further calculation of the E-field, T1-weighted and T2* images were acquired with following parameters: T1 MPRAGE sequence with 176 sagittal slices, matrix size = 256 × 240, voxel size = 1 × 1 × 1 mm^3, flip angle 9°, TR/TE/TI = 2300/2.98/900ms; T2* with 192 sagittal slices, matrix size = 512 × 512, voxel size = 0.488 × 0.488 × 1 mm^3, flip angle 120°, TR/TE = 5000/394 ms. The T1-weighted image was also used for neuronavigation during TMS. Diffusion MRI with 88 axial slices, matrix size = 128 × 128, voxel size = 1.719 × 1.719× 1.7 mm^3, TR/TE = 80/6000 ms, flip angle 90°, 67 diffusion directions, b-value 1000 s/mm^3 was acquired for the estimation of the conductivity anisotropy in the WM.

The individual activation map of attentional processing was measured by an event-related fMRI design based on the gradient echo planar (GE-EPI) sequence (60 axial slices, matrix size = 102 × 102, voxel size = 2 × 2 × 2.26 mm^3, flip angle 80°, TR/TE = 2000/24 ms, 775 volumes). Participants were instructed to perform the Posner task that required spatially congruent button presses in response to visual target stimuli.

2.4. MRI data analysis

2.4.1. Preprocessing

MRI data were preprocessed with fMRIPrep 20.1.1 (Esteban et al., 2019), a robust preprocessing pipeline based on Nipype 1.5.0 (Gorgolewski et al., 2011). The individual T1 image was first intensity corrected using N4BiasFieldCorrection (Tustison et al., 2010) and skull-stripped with antsBrainExtraction workflow. Brain tissue segmentation of GM, WM, and CSF was performed on the brain-extracted T1w using FSL FIRST 5.0.9 (Zhang et al., 2001). Brain surfaces were reconstructed using recon-all from FreeSurfer v6.0.1 (Dale et al., 1999), and the brain mask was refined with a custom variation of the Mindboggle method (Klein et al., 2017) to reconcile ANTs-derived and FreeSurfer-derived segmentations of the cortical gray matter. Volume-based spatial normalization to the MNI152Lin standard space was performed through nonlinear registration with the antsRegistration (ANTs 2.2.0).

Functional data were motion corrected using mcflirt (FSL 5.0.9) (Jenkinson et al., 2002) and slice-time corrected with 3dTshift from AFNI 20160207 (Cox and Hyde, 1997). Distortion correction was performed by 3dQwarp from the AFNI toolbox. The BOLD time series were then co-registered to the T1w reference using bbregister (FreeSurfer),

which implements boundary-based registration (Greve and Fischl, 2009), and resampled into the standard MNI152Lin space by antsApplyTransforms (ANTs). Finally, AFNI 3dmerge was used to spatially smooth the functional data with 6 mm full-width half-maximum Gaussian kernel.

Several motion-induced confounding regressors were also collected based on the preprocessed BOLD: six corresponding rotation and translation parameters, and framewise displacement (FD) (Power et al., 2014).

2.4.2. Activation analysis

Preprocessed data were analyzed with SPM 12 (Wellcome Department of Imaging Neuroscience, London, UK, http://www.fil.ion.ucl.ac.uk/spm). In the first level analysis, a general linear model (GLM) was generated to estimate task-related neural activities. This consists of three regressors of interest: valid, invalid, neutral, and one regressor of no interest: incorrect or missed responses. These regressors were time-locked to the target onset and modeled with a canonical synthetic haemodynamic response function (HRF) with duration of 0 s. Additionally, six motion regressors and one volume-masking regressor per FD value above 0.9 (Power et al., 2012) were added to regress out motion-induced artifacts. Trials with RT less than 100 ms or greater than 1000 ms were discarded as incorrect responses (Small et al., 2003).

On the second level, two t-contrasts were computed to identify areas preferentially engaged in attentional orienting/benefits (valid vs. neutral trials) and reorienting (invalid vs. valid trials), respectively. The contrast of valid vs. neutral trials isolates brain areas activated in trials with targets appearing at the attended position compared to no spatial expectation. The contrast between invalid and valid trials isolates areas activated by targets appearing at the unattended position after a directional spatial expectation was induced by the cue. False discovery rate (FDR) was used to avoid the bias of multiple comparisons (Benjamini and Hochberg, 1995) with $q = 0.05$. Individual peak activation coordinates of invalid > valid on rIPL were extracted to define the cortical area of interest in the subsequent TMS experiment. The Julich brain atlas (Amunts et al., 2020) was used to define the rIPL mask, which comprises one rostral (PGp) and one caudal (PGa) region in the angular gyrus (AG), and five regions of the supramarginal gyrus (SMG) (PFm, PF, PFop, PGcm, PFt).

2.5. TMS localization experiment

Seventeen of the 30 fMRI participants underwent an online TMS experiment while performing the Posner-like task (Figure 1b). TMS pulses were applied with coil positions over the larger rIPL area using a MagPro X100 stimulator (MagVenture,

firmware version 7.1.1) and an MCF-B65 figure-of-eight coil. Coil positioning was guided by a neuronavigation system (TMS Navigator, Localite, Germany, Sankt Augustin; camera: Polaris Spectra, NDI, Canada, Waterloo). The electromyographic (EMG) signal was amplified with a patient amplifier system (D-360, DigitimerLtd., UK, Welwyn Garden City; bandpass filtered from 10 Hz to 2 kHz) and recorded with an acquisition interface (Power1401 MK-II, CED Ltd., UK, Cambridge, 4 kHz sampling rate) and Signal (CED Ltd., version 4.11).

To determine the optimal stimulation intensity, we manually measured the resting motor threshold (rMT) of the participants' right index fingers with one surface electrode positioned over the first dorsal interosseous (FDI) muscle belly and one at the proximal interphalangeal joint (PIP). The rMT was defined as the minimum stimulator intensity to induce a motor-evoked potential (MEP) larger than 50 μV in at least 5 of 10 consecutive trials (Beynel et al., 2019).

500 bursts of rTMS with 5 pulses at 10 Hz each were applied at 100% rMT (Beynel et al., 2019, Rushworth et al., 2001) during the 500 Posner-like task trials, comprising 375 *valid* trials (75%) and 125 *invalid* trials (25%). After every 100 trials, a short break of ~2 min was advised to avoid fatigue. The bursts were initiated 20 ms after target presentation to disrupt attentional processing transiently (Figure 1b). We restricted the area over which the coil centers were located to a circular zone of 3 cm radius around the individual fMRI-derived activation peak (invalid > valid trials) in the rIPL. Stimulation area centers were moved 2 cm anterior/superior in 4 subjects because their activation peaks were close to the occipital or temporal lobe. Coil positions and orientations were randomly selected within the defined circular zone for each burst, to increase electric field variability by minimizing cross-correlations between induced electric fields (Numssen et al., 2021b). Note that eleven participants were sampled with a "quadrant mode": we randomly sampled 100 stimulations for each quadrant of the stimulation area, resulting in 400 trials. The final 100 trials were arbitrarily attributed across the whole stimulation area. To diminish possible sequential effects, we used a "random mode" for the remaining six participants: all 500 trials were randomly sampled throughout the experimental session. Coil positions and corresponding behavioral responses, i.e., reaction time and accuracy, were recorded for each trial.

2.6. TMS mapping

2.6.1. Numerical simulations of the induced electric field

Individual head models were reconstructed using the headreco pipeline (Nielsen et al., 2018) utilizing SPM12 and CAT12 (http://www.neuro.uni-jena.de/cat/) for all seventeen

subjects. The final head models were composed of approximately 3.4 × 10^6 nodes and 20 × 10^6 tetrahedra (average volume: approximately 0.15 mm^3 in the cortex). Seven tissue types were included with standard conductivity estimates: white matter (σ_{WM} = 0.126 S/m), gray matter (σ_{GM} = 0.275 S/m), cerebrospinal fluid (σ_{CSF} = 1.654 S/m), bone (σ_B = 0.01 S/m), skin (σ_S = 0. 465 S/m), ventricle (σ_V = 1.654 S/m) and eyeballs (σ_{EB} = 0.5 S/m) (Thielscher et al., 2015, Wagner et al., 2004). WM and GM were assigned anisotropic conductivities while the five other tissues were treated as isotropic. Electric fields induced by coil positions of all TMS trials were then computed considering individual head geometry and employing the FEM-based solver implemented in SimNIBS v3.2.6 (Saturnino et al., 2019, Thielscher et al., 2015). See Saturnino et al. (2019) for more details on the numerical simulation.

A refined region of interest (ROI) was defined around the rIPL area based on the Julich brain atlas (Amunts et al., 2020) to improve the numerical resolution around the selected ROI. All analyses were performed on the midlayer between GM and WM surfaces to avoid boundary effects of E-field due to conductivity discontinuities.

2.6.2. Regression analysis

The regression approach used in this study is based on a recently developed modeling framework in the motor cortex (Numssen et al., 2021b, Weise et al., 2022, Weise et al., 2020). The principal idea of the regression approach is to combine the outcome of multiple stimulation experiments with the induced E-fields of different coil positions and orientations, assuming that, at the effective site, the relationship between E-field and behavioral performance is stable, i.e., the same electric field strength always evokes the same behavioral output. In particular, the method leverages more information by simultaneously varying both coil positions and orientations exploiting electric field variability to avoid bias towards locations with high E-field magnitudes, such as the gyral crown.

We first discarded TMS trials with RT < 100 ms or RT > 1000 ms, and those with a coil distance ≥ 5 mm from the skin surface. Subsequently, the valid trials were randomly downsampled to the number of invalid trials to guard against potential sample-size-dependent effects. In addition, any linear trends of RT over time were removed to mitigate potential learning or fatigue effects.

After data cleaning, we performed Linear regression analysis to identify the neural populations that are causally involved in attentional processing for every element within the ROI (Weise et al., 2020). The linear relationship between E-field magnitude $x_{i,j}$ of TMS trial i ($1 \leq i \leq N_{TMS}$) at the cortical element j ($1 \leq j \leq N_{elms}$) and the

estimated RT $\hat{y}_{i,j}$ is calculated:

$$\hat{y}_{i,j} = \alpha_j + \beta_j x_{i,j}$$

Here, α is the intercept and β is the slope.

The site of effective stimulation can be quantified by the goodness-of-fit (GOF), which would be highest at the cortical site that houses the relevant neuronal populations (Numssen et al., 2021b). We assessed the element-wise GOF by the coefficient of determination R^2:

$$R_j^2 = 1 - \frac{VAR\ (y - \hat{y}_j)}{VAR\ (y)}$$

Where y is the measured RT. Higher R^2 denotes better fitting results.

The regression analysis was applied separately to invalid and valid trials and yielded one R^2 score per ROI element. We dropped all negative R^2 values as these denote areas of poor fitting. We then multiplied the raw R^2 value with the slope's sign to include not only the goodness of fit (R^2) but also the direction of the TMS effect in one metric:

$$\widetilde{R_j^2} = R_j^2 \cdot \text{sign}\ (\beta_j)$$

This allowed us to visually differentiate cortical areas of inhibitory TMS effects (positive slope areas) from areas of facilitatory TMS effects (negative slope areas).

We intended to compare the anatomical locations between the sites of highest $\widetilde{R_j^2}$ and the individual fMRI peak, and we assumed that high-frequency rTMS on rIPL will selectively impair invalid trials, resulting in higher $\widetilde{R_j^2}$ values compared to valid trials.

To generate the group $\widetilde{R^2}$ map, all individual $\widetilde{R^2}$ maps were first mapped to the group averaged brain template, then voxel-wise $\widetilde{R^2}$ values were averaged across subjects.

3. Results

3.1. Behavioral performance

Behavioral results from the fMRI experiment showed a reliable difference of RT between conditions ($F_{2,87}$ = 5.38, p < 0.01; invalid$_{fMRI}$: 403 ms $\pm$ 69 ms; valid$_{fMRI}$: 345 ms $\pm$ 70 ms; neutral$_{fMRI}$: 384 ms $\pm$ 72 ms). Post-hoc t-tests confirmed a reorienting effect, that is, slower RTs for invalid compared to valid targets (t_{29} = 15.25, p < 0.01). There was no significant difference between neutral and valid or invalid trials (Figure 2a). No significant differences were found in accuracy ($F_{2,87}$ = 0.92, p = 0.40; invalid$_{fMRI}$: 0.95 $\pm$ 0.08, valid$_{fMRI}$: 0.97 $\pm$ 0.06, neutral$_{fMRII}$: 0.95 $\pm$ 0.06).

In the TMS experiment, we again found a significantly slower response speed for invalid relative to valid trials (t_{16} = 12.69, p < 0.01; invalid$_{TMS}$: 336 ms ± 62 ms; valid$_{TMS}$: 266 ms ± 61 ms). In line with our hypothesis, task accuracy was also significantly decreased in the invalid condition (t_{16} = 4.10, p < 0.01; invalid$_{TMS}$: 0.93 ± 0.06; valid$_{TMS}$: 0.98 ± 0.02) (Figure 2b).

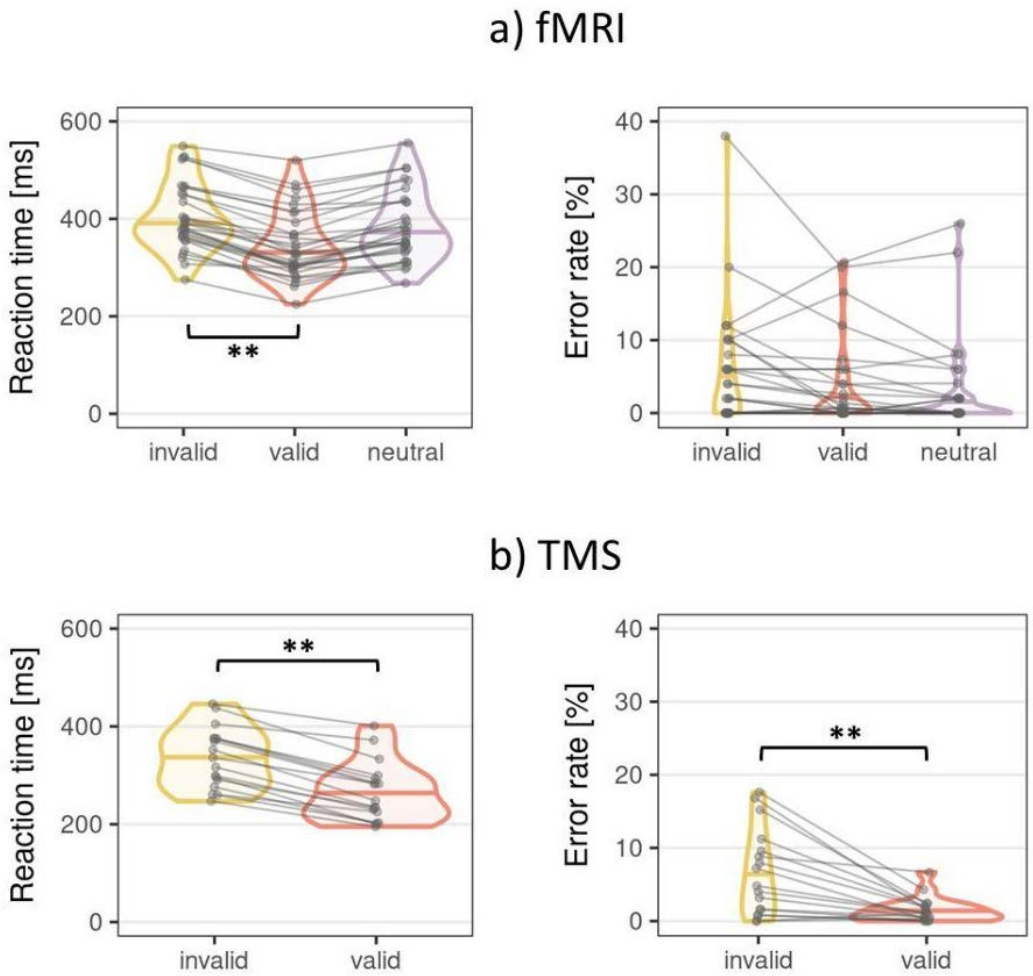

Figure 2. Behavioral results of the Posner task during fMRI and TMS. Reorienting attention (*invalid* trials) was significantly slower than attentional orientation (*valid* trials), both in the fMRI (a) and in the TMS (b) realization. For task accuracy, significant differences were only present during TMS. ** p < 0.01. Grey points/lines: single subjects.

3.2. fMRI activation

The fMRI results revealed distributed bilateral brain regions from different networks for the reorienting of attention (Figure 3a). These include the ventral attention network (IPL, MFG), the dorsal attention network (SPL, FEF), and the salience network (Insula; anterior cingulate cortex, ACC). In contrast, the default mode network (DMN) (posterior

cingulate cortex, PCC; medial prefrontal cortex, mPFC) was deactivated for invalid relative to valid trials. These findings go beyond the classic view of a ventral, right-lateralized reorientation system. Relative to the neutral condition, attentional orienting showed deactivation of both IPS and SPL, but increased activation of mPFC (Figure 3b). All activations are reported at the level of q = 0.05 after FDR correction.

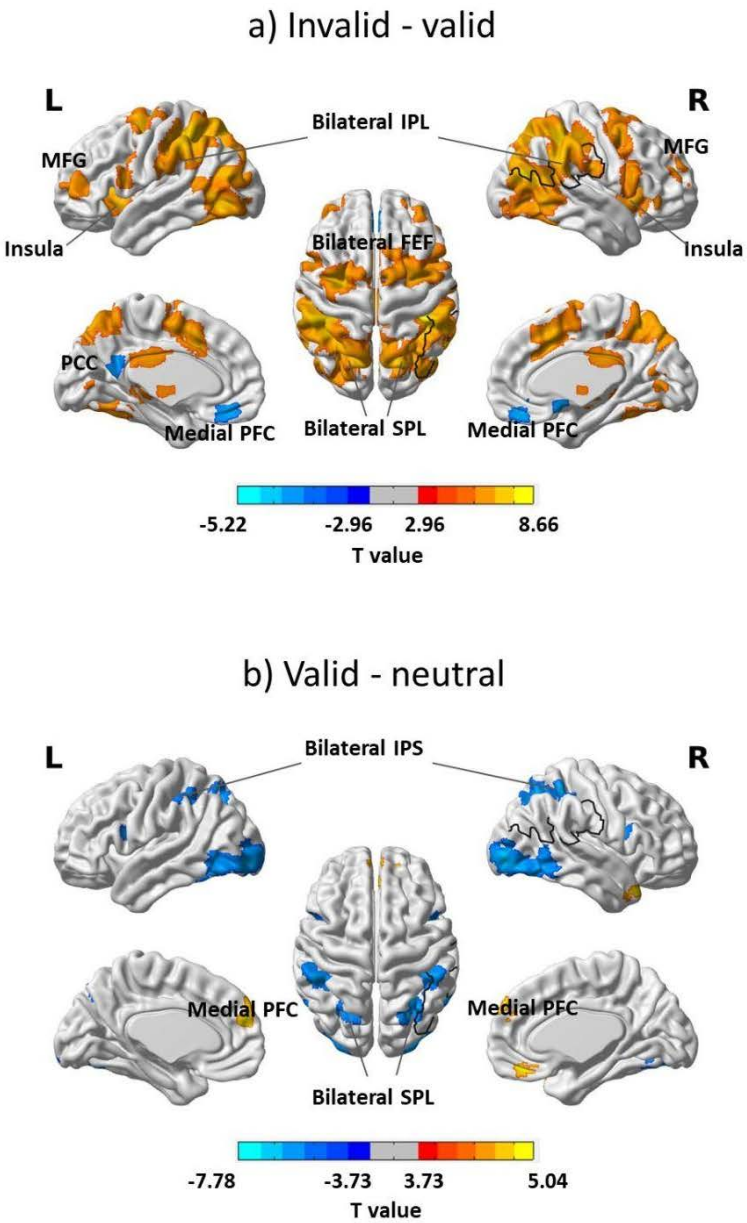

Figure 3. Spatial attention recruits distributed networks: fMRI activation results during attentional orientation and reorientation. (a) Relative to valid trials, the invalid condition exhibits significant activation in both dorsal and ventral attention networks, and salience network. (b) Attentional orientation resulted in increased activation of medial prefrontal cortex and deactivation of parietal areas (FDR correction, q = 0.05).

3.3. TMS mapping results

At the group level, the relationship between the induced E-field and the behavioral modulation differed significantly between valid and invalid trial types (Figure 6). Specifically, the group-level $\widetilde{R^2}$ maps for the invalid condition were dominated by positive relationships, i.e., higher E-field leads to a slower response, implying a perturbation effect on the invalid condition. On the contrary, the group-level $\widetilde{R^2}$ map for the valid condition was close to zero indicating that there was no effect of TMS for attentional orientation (Figure 5).

In Figure 4, we present results for a representative subject with moderate fitting results to show the linear regression maps from prominent locations. As shown at three elements (one with the highest GOF of negative linear trend, one on the activation peak, and one with the highest GOF of positive linear trend), the correlation between measured RTs and the computed E-fields did not show a clear S-shaped curve, as MEP data did (Numssen et al., 2021b, Weise et al., 2020)

Figure 5 shows group-averaged (green background) and single-subject results from all seventeen individuals, both for the TMS and the fMRI study. Pink background denotes the “quadrant sampling mode” and cyan background represents the “random sampling mode”. For the group averaged $\widetilde{R^2}$ map, the invalid and valid conditions exhibit different patterns. In the invalid condition, most of the cortical regions, especially in the SMG, show a positive correlation, indicating a delayed response speed with increased E-field exposure, while there is no obvious pattern for valid trials. The group-level results align with our hypothesis that TMS should selectively exert a perturbative effect on attentional reorientation without affecting the initial attentional orientation. TMS mapping and fMRI activation results identify similar cortical areas for attentional processes especially in subjects with prominent recruitment of the rIPL for attentional processes, e.g., subject 01, 03, and 06.

In terms of magnitude of $\widetilde{R^2}$, Table 1 shows the individual maximum $\widetilde{R^2}$ scores for the invalid and valid conditions. Given that the TMS basically revealed an inhibitory effect on attentional processing, we only presented $\widetilde{R^2}$ scores that shows positive correlation between E-field and RT in Table 1. A Wilcoxon signed rank test revealed a significant difference of the maximum $\widetilde{R^2}$ between the two conditions (Z = 2.273, p < 0.05; $\widetilde{R^2}_{invalid}$= 0.066 $\pm$ 0.037, $\widetilde{R^2}_{valid}$ = 0.037 $\pm$ 0.022) (Figure 6). Compared with the valid condition, the $\widetilde{R^2}$ values are higher in the invalid condition, identifying a stronger disruptive effect of the E-field on the response speed during attentional reorienting.

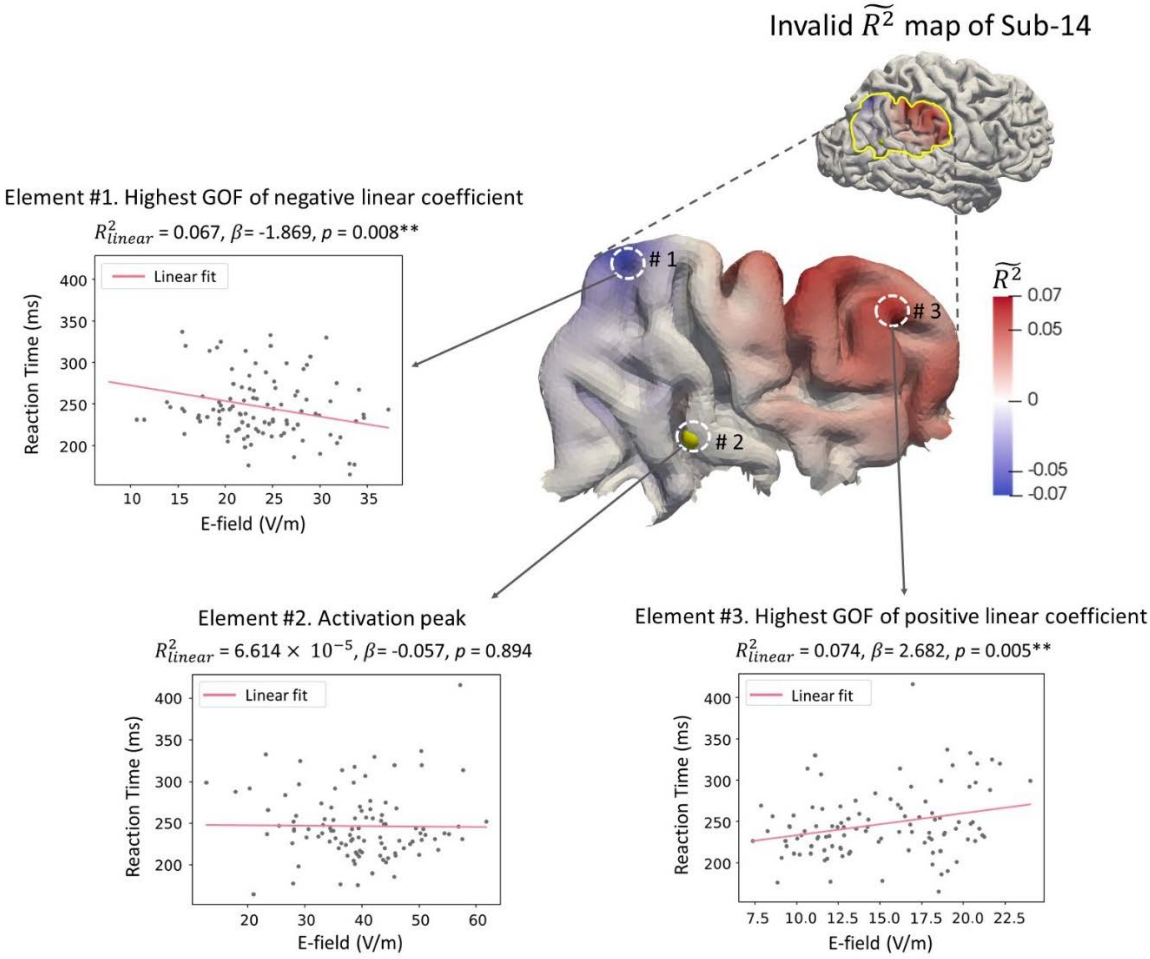

Figure 4. TMS-induced modulation of attentional reorientation from one representative subject with moderate GOF (sub-14). The $\widetilde{R^2}$ map is derived from voxel-wise linear regression of invalid trials, multiplied with the sign of slope to include information about inhibitory (positive slope values) versus facilitatory TMS effects (negative TMS values). The linear fitting lines are shown for 3 elements: #1 with the highest GOF of negative linear correlation, #2 is the fMRI activation peak of reorientation, and #3 with the highest GOF of positive linear correlation. The yellow sphere embedded in the gyral crown marks the location of fMRI activation peak. β denotes the slope of linear regression, and p values are the significant level of β. **: $p < 0.01$. Grey points: single TMS trials.

Table 1. Individual activation peaks and TMS results.

Subject ID	Activation peak	MT	Invalid $\widetilde{R^2}_{max}$	Valid $\widetilde{R^2}_{max}$
01	(56, -37, 34)	43%	0.055	0.028
02	(42, -55, 50)	39%	0.056	0.082
03	(60, -41, 31)	70%	0.059	0.025
04	(54, -33, 34)	47%	0.040	0.034
05	(54, -61, 18)	57%	0.126	0.063
06	(62, -57, 34)	64%	0.084	0.034
07	(52, -53, 16)	46%	0.013	0.031
08	(42, -73, 40)	43%	0.030	0.062
09	(56, -63, 25)	45%	0.039	0.078
10	(58, -47, 36)	45%	0.037	0.011
11	(46, -69, 20)	42%	0.073	0.035
12	(69, -39, 34)	53%	0.152	0.012
13	(52, -51, 31)	56%	0.071	0.011
14	(54, -67, 27)	38%	0.074	0.015
15	(42, -77, 29)	40%	0.117	0.024
16	(56, -67, 34)	52%	0.045	0.040
17	(58, -47, 50)	44%	0.045	0.039
Group average	(51, -55, 32)	48%	0.066	0.037

Notes: The Activation peak column provides individual fMRI peak coordinates in the rIPL for the invalid-valid contrast in standard MNI space. The individual resting motor threshold (MT) is provided in the percentage of maximum stimulator output (% MSO), and the maximum $\widetilde{R^2}$, both for invalid and valid conditions with positive correlation between E-field and RT.

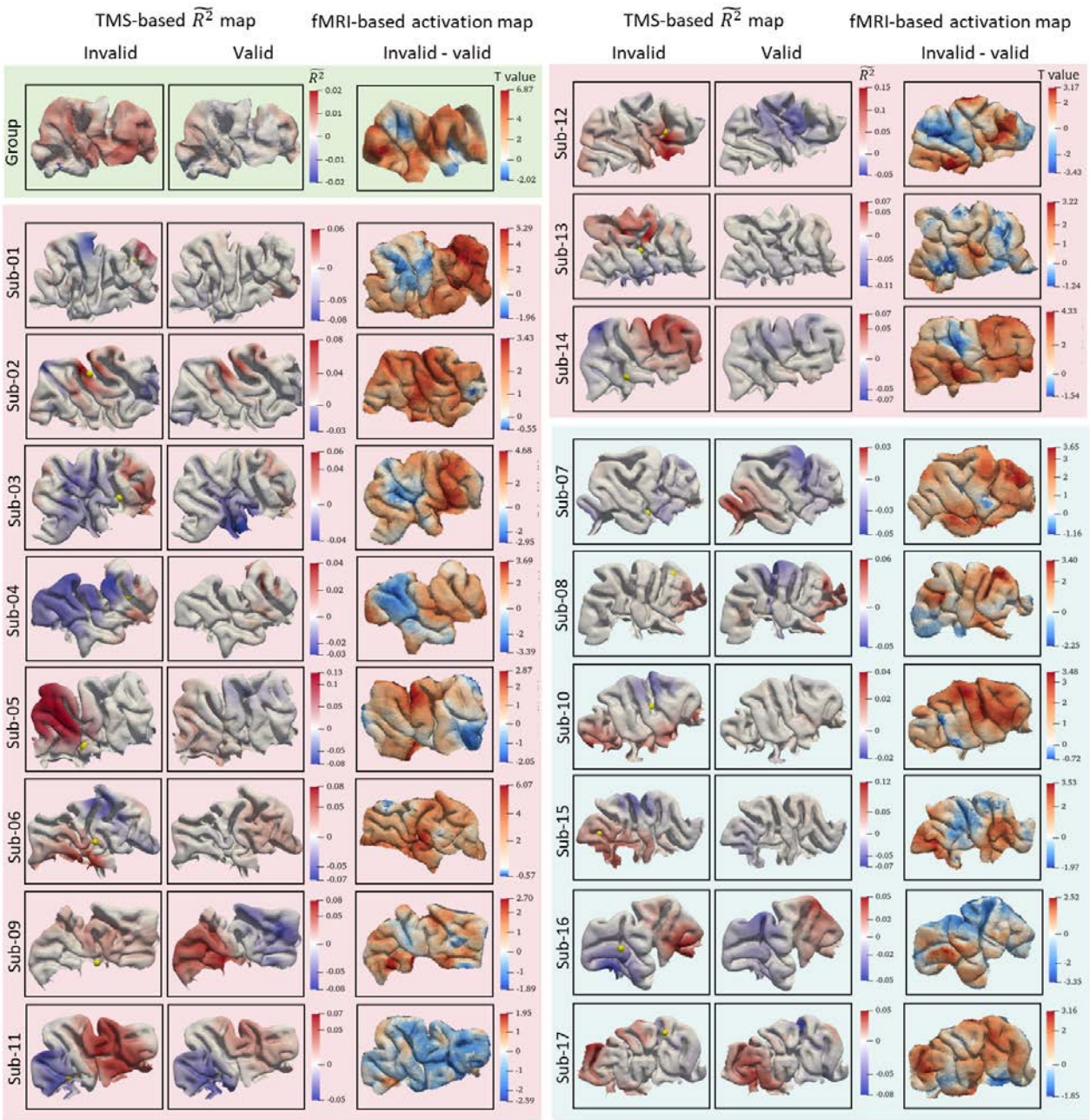

Figure 5. Inhibitory TMS effects on attentional reorientation are subject-specific. This figure shows the group (green background) and individual $\widetilde{R^2}$ maps (pink and cyan background) on the rIPL, as well as the corresponding activation maps. $\widetilde{R^2}$ maps were generated by R^2 scores multiplied with the slope's sign to represent the direction information of the linear correlation. Pink background color codes subjects sampled with "quadrant mode", while cyan color denotes "random sampling mode" (see text). Yellow spheres in the invalid column represent the fMRI activation peak location of the invalid-valid contrast. Note that the $\widetilde{R^2}$ scores were mapped onto the midlayer surface between white and grey matter whereas the fMRI activation results are mapped onto the cortical grey matter surface. The group rIPL map for $\widetilde{R^2}$ scores were derived from the averaged surface of our seventeen subjects, whereas the group activation map was based on fsaverage template.

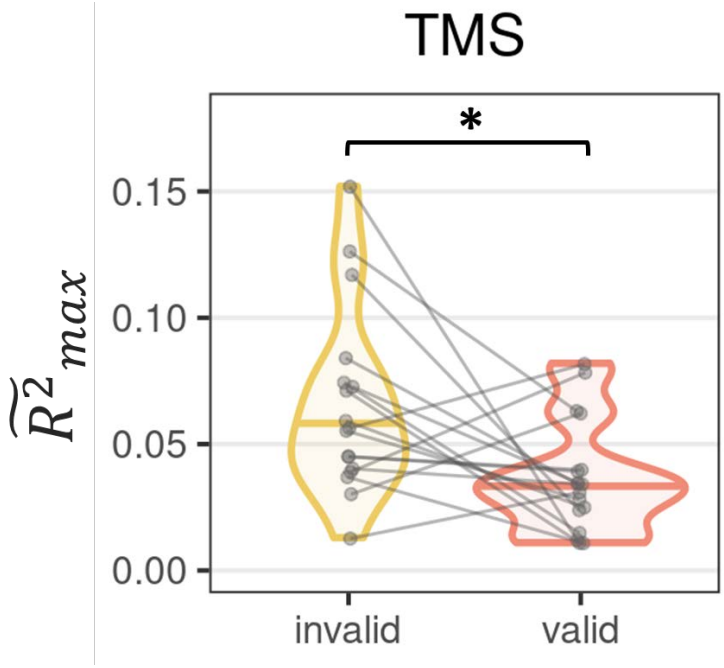

Figure 6. TMS selectively affects attentional reorienting. Invalid trials (reflecting attentional reorienting) were significantly stronger related to the induced E-field than valid trials (reflecting attentional orientation). *: $p < 0.05$. Grey points/lines: single subjects.

4. Discussion

We applied our previously established regression approach (Numssen et al., 2021b) to localize the neuronal underpinnings of attentional processes with TMS. In this statistical approach, cortical stimulation exposure across multiple stimulation sites is related to the TMS-induced change in behavior. Here, we studied the relation between the strength of TMS-induced E-field in the cortex and the inhibitory effects of TMS on spatial attention, to identify the relevant cortical regions for attentional processing within the rIPL. On the group level, we found a task-specific inhibitory TMS effect on attentional reorienting, but not on attentional orienting. This effect was particularly pronounced for stimulating the SMG within the larger rIPL region. On the single-subject level, the regression analyses identified large individual variability, both for the cortical organization as well as for TMS responsiveness. In addition, we identified differences in BOLD-measured neuronal activity and TMS-evoked neuronal effects. This incongruence highlights the principal distinction between neural activity being correlated with (or maybe even caused by) particular paradigms, and activity of neural populations exercising a causal influence on the behavioral outcome.

fMRI results. The ability to orient attention is a fundamental component of most perceptual-motor processes in everyday life (Natale et al., 2009). Consequently, we took our first step in generalizing the regression method to spatial attention. Spatial

orienting can be driven either endogenously, by predictive contingencies, i.e., top-down cues, or exogenously, by unexpected bottom-up signals stemming for example from visual inputs. These processes are accomplished by the interaction of several cortical regions, forming functional networks (Chica et al., 2011). Our fMRI results show that large-scale brain networks were activated during attentional reorienting, including both dorsal and ventral attention networks, which reflects the neural bases of the interplay between these two attention mechanisms (Shulman et al., 2009, Proskovec et al., 2018). One of these regions, the rIPL, is consistently identified as a major network hub in diverse cognitive functions, from bottom-up perception to higher cognitive capacities that are unique for humans (Cabeza et al., 2012, Igelström and Graziano, 2017). It is worth noting that we found bilateral IPL and VFC activated when participants attempted to process the target at an unexpected location, which challenges the traditional view that the VAN is lateralized to the right hemisphere (Lunven and Bartolomeo, 2017). The comparison of attentional orientation and neutral trials (valid - neutral) allowed us to separate attentional benefits from visual, motor, or other basic cognitive tasks (i.e., valid - baseline), and to explore the influence of cue predictiveness on spatial attention. Previous studies could not provide conclusive explanations for this effect of top-down predictions. Some researchers observed significant activation for valid minus neutral trials in either DAN or VAN (Peelen et al., 2004, Natale et al., 2009), while others found a significant deactivation of the rIPL when participants are orienting their attention to the predictive cues (Doricchi et al., 2010). Our results show that, when attention was focused on the valid side, bilateral IPS and SPL were suppressed, potentially to prevent reorienting to distracting events. Specifically, activation of medial PFC as a part of DMN may indicate an endogenous focus.

TMS localization. We performed state-of-the-art FEM-based E-field simulations to allow for realistic quantifications of the effect of cortical stimulation on attentional processes. TMS led to an interference effect on attentional processing, which is in line with our hypothesis that TMS on rIPL should selectively perturb the reorientation of attention (Rushworth et al., 2001). This specificity of the TMS effect is reflected in robust relationships between E-field exposure and behavioral modulation for attentional reorientation, but not attentional orientation. In general, the TMS-induced effect, measured by the coefficient of determination $\widetilde{R^2}$, was much lower for attention as compared to the motor domain, in which the TMS regression approach was previously established (Numssen et al., 2021b, Weise et al., 2020). Lower $\widetilde{R^2}$ values likely reflect the more restricted impact of the E-field on reaction time compared to its

effect on muscle recruitment when stimulating the primary motor cortex.

In fact, TMS studies with cognitive paradigms often show high inter-individual variability and results are not always conclusive (Bergmann and Hartwigsen, 2021). Moreover, some cognitive paradigms suffer from relatively low test-retest reliability which may contribute to the strong variability of behavioral results (Hedge et al., 2018). The key problem is that the underlying neural basis of cognitive functions is much more complex and variable than that of eliciting hand muscle twitches (Fetsch, 2016). In our study, in spite of this high variability, we were still able to distill out the TMS effect on attentional reorienting. However, the large amount of residual variance indicates that taking into account additional variables and more complex models (multivariate regression) is likely to improve accuracy and reliability.

TMS vs. fMRI localization. We paralleled the fMRI-based activation maps with TMS-based cortical mapping to explore the gains of regression-based functional TMS mappings in the domain of higher cognition. Behavioral results showed that rTMS over the rIPL impaired attentional reorientation, leading to increased response latencies and decreased task accuracy. Group-level analyses of the TMS-based mapping refined this disruptive TMS-effect to the SMG, the anterior part of the IPL. Of note, the rIPL is a large region that comprises two major gyri: SMG and AG, separated by the intermediate sulcus of Jensen (Segal and Petrides, 2012). Previous studies suggested that both SMG and AG are critical for attention shifts between visual stimuli (Chambers et al., 2004). fMRI results consistently found that in response to invalid cues, activation peaks are located either in the AG or SMG (Decety and Lamm, 2007). A behavioral and functional connectivity-based meta-analysis further defined the functional topography of rIPL (Wang et al., 2016). They revealed that the SMG primarily participates in attention, execution, and action inhibition, while the AG is involved in social and spatial cognition. In line with our group averaged $\widetilde{R^2}$ map results, these findings may reflect the crucial role of the right SMG in attentional reorientation.

Transferring the TMS regression approach to the study of higher cognition. The TMS regression approach integrates information from multiple stimulation patterns to map structure-function relationships based on the causal effect of the induced electric field. The main metric to separate cortical locations is the explained variance of the behavioral modulation ($\widetilde{R^2}$). The explained variance was significantly higher for attentional reorientation compared to attentional orientation. However, applying the regression approach to the motor domain (Numssen et al., 2021b) explained distinctively higher levels of variance (10% vs 80% in single subjects). These

comparatively low $\widetilde{R^2}$ values for attentional orientation processes most probably stem from several sources: Firstly, behavioral responses to higher cognitive tasks, such as the Posner task, intrinsically exert higher variance due to complex processing demands (Hedge et al., 2018) that give rise to confounding factors, such as fatigue or mental state. Secondly, task processing is spread considerably across the cortex, in contrast to very focal representations within the motor system. For any coil position, a multitude of cortical locations are stimulated which, independently or in interaction with each other, exercise an influence on the outcome variable (here, attentional reorienting). The organization of the rIPL is challenging to study due to the complex anatomy and highly divergent functional segregation of this cortical region (Williams et al., 2022, Krall et al., 2016). The TMS trials with different coil positions/orientations may differentially target cortical sites that have various functions. Some of the varying targets can accumulate together and thus exert inhibitory or excitatory effects, others might neutralize the TMS effect. Previous studies confirmed that compared to single-node TMS, the concurrent frontal-parietal network TMS showed a reduction of the reorienting effect in the right hemifield (Gallotto et al., 2022). Therefore, the network effect must be considered in future studies. One possibility into that direction would be the development of multivariate regression schemes. Finally, it should be noted that the interaction between internal factors such as the current brain state, fatigue and baseline performance level and external stimulation parameters such as intensity, frequency and duration is not well understood (Hartwigsen and Silvanto, 2022). Such interactions may induce strong inter-individual variability in response to TMS in studies of cognition. Nevertheless, we argue that transferring our TMS regression approach to cognitive domains will ultimately help to optimize TMS protocols.

5. Conclusion

To conclude, we successfully applied a TMS-based localization approach based on functional analyses of the induced E-fields and their behavioral modulation in a higher-cognitive domain. With this causal approach, we quantified TMS effects on attentional reorientation and highlighted, both, interindividual variation in cortical organization and differences between fMRI activity and TMS mapping. The results show that E-field modeling can play a valuable role when exploring structure-function relationships with non-invasive brain stimulation methods. We are positive that this approach of combining E-field modeling and behavioral modulation can be further generalized and applied to other functional domains to increase TMS effectiveness and allow its applications at the individual level. To increase the specificity and sensitivity of the method, we suggest developing multivariate regression approaches that account for

the recruitment of distributed networks by cognitive function relies upon, yielding multiple points of potential TMS influence. Moreover, the utilization of alternative readout variables, such as physiological (e.g., heart rate) and electrophysiological (e.g., TMS-evoked electroencephalogram potentials) measures, may increase the information gain of TMS mapping in cognitive schemes.

Acknowledgments

The authors would like to acknowledge the support from the German Research Foundation (grant no. HA 2899/31-1, HA 6314/9-1, KN 588/10-1 to JH, GH and TRK; and grant no. WE 59851/2 to KW). GH is supported by the Max Planck Society. YJ would also like to thank the China Scholarship Council for its financial support.

Declaration of interests

The authors declare no competing interests.

References

AMUNTS, K., MOHLBERG, H., BLUDAU, S. & ZILLES, K. 2020. Julich-Brain: A 3D probabilistic atlas of the human brain's cytoarchitecture. *Science,* 369**,** 988-992.

BENJAMINI, Y. & HOCHBERG, Y. 1995. Controlling the false discovery rate: a practical and powerful approach to multiple testing. *Journal of the Royal statistical society: series B,* 57**,** 289-300.

BERGMANN, T. O. & HARTWIGSEN, G. 2021. Inferring causality from noninvasive brain stimulation in cognitive neuroscience. *Journal of cognitive neuroscience,* 33**,** 195-225.

BESTMANN, S. & FEREDOES, E. 2013. Combined neurostimulation and neuroimaging in cognitive neuroscience: past, present, and future. *Annals of the New York Academy of Sciences,* 1296**,** 11-30.

BEYNEL, L., APPELBAUM, L. G., LUBER, B., CROWELL, C. A., HILBIG, S. A., LIM, W., NGUYEN, D., CHRAPLIWY, N. A., DAVIS, S. W. & CABEZA, R. 2019. Effects of online repetitive transcranial magnetic stimulation (rTMS) on cognitive processing: a meta-analysis and recommendations for future studies. *Neuroscience Biobehavioral Reviews* 107**,** 47-58.

BUNGERT, A., ANTUNES, A., ESPENHAHN, S. & THIELSCHER, A. 2017. Where does TMS stimulate the motor cortex? Combining electrophysiological measurements and realistic field estimates to reveal the affected cortex position. *Cerebral Cortex,* 27**,** 5083-5094.

CABEZA, R., CIARAMELLI, E. & MOSCOVITCH, M. 2012. Cognitive contributions of the ventral

parietal cortex: an integrative theoretical account. *Trends in cognitive sciences,* 16**,** 338-352.

CHAMBERS, C. D., STOKES, M. G. & MATTINGLEY, J. B. 2004. Modality-specific control of strategic spatial attention in parietal cortex. *Neuron,* 44**,** 925-930.

CHICA, A. B., BARTOLOMEO, P. & VALERO-CABRÉ, A. 2011. Dorsal and ventral parietal contributions to spatial orienting in the human brain. *Journal of Neuroscience,* 31**,** 8143-8149.

CORBETTA, M., PATEL, G. & SHULMAN, G. 2008. The reorienting system of the human brain: from environment to theory of mind. *Neuron,* 58**,** 306-324.

CORBETTA, M. & SHULMAN, G. L. 2002. Control of goal-directed and stimulus-driven attention in the brain. *Nature reviews neuroscience,* 3**,** 201-215.

COX, R. W. & HYDE, J. S. 1997. Software tools for analysis and visualization of fMRI data. *NMR in Biomedicine: An International Journal Devoted to the Development Application of Magnetic Resonance In Vivo,* 10**,** 171-178.

DALE, A. M., FISCHL, B. & SERENO, M. I. 1999. Cortical surface-based analysis: I. Segmentation and surface reconstruction. *Neuroimage,* 9**,** 179-194.

DECETY, J. & LAMM, C. 2007. The role of the right temporoparietal junction in social interaction: how low-level computational processes contribute to meta-cognition. *The neuroscientist,* 13**,** 580-593.

DORICCHI, F., MACCI, E., SILVETTI, M. & MACALUSO, E. 2010. Neural correlates of the spatial and expectancy components of endogenous and stimulus-driven orienting of attention in the Posner task. *Cerebral Cortex,* 20**,** 1574-1585.

ESTEBAN, O., MARKIEWICZ, C. J., BLAIR, R. W., MOODIE, C. A., ISIK, A. I., ERRAMUZPE, A., KENT, J. D., GONCALVES, M., DUPRE, E. & SNYDER, M. 2019. fMRIPrep: a robust preprocessing pipeline for functional MRI. *Nature methods,* 16**,** 111-116.

FETSCH, C. R. 2016. The importance of task design and behavioral control for understanding the neural basis of cognitive functions. *Current opinion in neurobiology,* 37**,** 16-22.

GALLOTTO, S., SCHUHMANN, T., DUECKER, F., MIDDAG-VAN SPANJE, M., DE GRAAF, T. A. & SACK, A. T. 2022. Concurrent frontal and parietal network TMS for modulating attention. *Iscience,* 25**,** 103962.

GORGOLEWSKI, K., BURNS, C. D., MADISON, C., CLARK, D., HALCHENKO, Y. O., WASKOM, M. L. & GHOSH, S. S. 2011. Nipype: a flexible, lightweight and extensible neuroimaging data processing framework in python. *Frontiers in neuroinformatics***,** 13.

GREVE, D. N. & FISCHL, B. 2009. Accurate and robust brain image alignment using boundary-

based registration. *Neuroimage,* 48**,** 63-72.

GROPPA, S., MUTHURAMAN, M., OTTO, B., DEUSCHL, G., SIEBNER, H. R. & RAETHJEN, J. 2013. Subcortical substrates of TMS induced modulation of the cortico-cortical connectivity. *Brain stimulation,* 6**,** 138-146.

GROSBRAS, M.-H. & PAUS, T. 2002. Transcranial magnetic stimulation of the human frontal eye field: effects on visual perception and attention. *Journal of cognitive neuroscience,* 14**,** 1109-1120.

HALLETT, M. 2000. Transcranial magnetic stimulation and the human brain. *Nature,* 406**,** 147-150.

HARTWIGSEN, G., BERGMANN, T. O., HERZ, D. M., ANGSTMANN, S., KARABANOV, A., RAFFIN, E., THIELSCHER, A. & SIEBNER, H. R. 2015. Modeling the effects of noninvasive transcranial brain stimulation at the biophysical, network, and cognitive level. *Progress in brain research,* 222**,** 261-287.

HARTWIGSEN, G. & SILVANTO, J. 2022. Noninvasive Brain Stimulation: Multiple Effects on Cognition. *The Neuroscientist***,** 10738584221113806.

HEDGE, C., POWELL, G. & SUMNER, P. 2018. The reliability paradox: Why robust cognitive tasks do not produce reliable individual differences. *Behavior research methods,* 50**,** 1166-1186.

IGELSTRÖM, K. M. & GRAZIANO, M. S. 2017. The inferior parietal lobule and temporoparietal junction: a network perspective. *Neuropsychologia,* 105**,** 70-83.

JENKINSON, M., BANNISTER, P., BRADY, M. & SMITH, S. 2002. Improved optimization for the robust and accurate linear registration and motion correction of brain images. *Neuroimage,* 17**,** 825-841.

JOHNSON, A. & PROCTOR, R. W. 2004. *Attention: Theory and practice*, Sage.

KLEIN, A., GHOSH, S. S., BAO, F. S., GIARD, J., HÄME, Y., STAVSKY, E., LEE, N., ROSSA, B., REUTER, M. & CHAIBUB NETO, E. 2017. Mindboggling morphometry of human brains. *PLoS computational biology,* 13**,** e1005350.

KRALL, S. C., VOLZ, L. J., OBERWELLAND, E., GREFKES, C., FINK, G. R. & KONRAD, K. 2016. The right temporoparietal junction in attention and social interaction: A transcranial magnetic stimulation study. *Human brain mapping,* 37**,** 796-807.

LAAKSO, I., MURAKAMI, T., HIRATA, A. & UGAWA, Y. 2018. Where and what TMS activates: experiments and modeling. *Brain Stimulation,* 11**,** 166-174.

LUNVEN, M. & BARTOLOMEO, P. 2017. Attention and spatial cognition: Neural and anatomical substrates of visual neglect. *Annals of physical rehabilitation medicine*

60, 124-129.

NATALE, E., MARZI, C. A. & MACALUSO, E. 2009. FMRI correlates of visuo-spatial reorienting investigated with an attention shifting double-cue paradigm. *Human Brain Mapping,* 30, 2367-2381.

NIELSEN, J. D., MADSEN, K. H., PUONTI, O., SIEBNER, H. R., BAUER, C., MADSEN, C. G., SATURNINO, G. B. & THIELSCHER, A. 2018. Automatic skull segmentation from MR images for realistic volume conductor models of the head: Assessment of the state-of-the-art. *Neuroimage,* 174, 587-598.

NIEMINEN, J. O., KOPONEN, L. M. & ILMONIEMI, R. J. 2015. Experimental characterization of the electric field distribution induced by TMS devices. *Brain stimulation,* 8, 582-589.

NUMSSEN, O., BZDOK, D. & HARTWIGSEN, G. 2021a. Functional specialization within the inferior parietal lobes across cognitive domains. *elife,* 10.

NUMSSEN, O., ZIER, A.-L., THIELSCHER, A., HARTWIGSEN, G., KNÖSCHE, T. R. & WEISE, K. 2021b. Efficient high-resolution TMS mapping of the human motor cortex by nonlinear regression. *NeuroImage,* 245, 118654.

PEELEN, M. V., HESLENFELD, D. J. & THEEUWES, J. 2004. Endogenous and exogenous attention shifts are mediated by the same large-scale neural network. *Neuroimage,* 22, 822-830.

PERERA, T., GEORGE, M. S., GRAMMER, G., JANICAK, P. G., PASCUAL-LEONE, A. & WIRECKI, T. S. 2016. The clinical TMS society consensus review and treatment recommendations for TMS therapy for major depressive disorder. *Brain stimulation,* 9, 336-346.

POSNER, M. I. 1980. Orienting of attention. *Quarterly journal of experimental psychology,* 32, 3-25.

POWER, J. D., BARNES, K. A., SNYDER, A. Z., SCHLAGGAR, B. L. & PETERSEN, S. E. 2012. Spurious but systematic correlations in functional connectivity MRI networks arise from subject motion. *Neuroimage,* 59, 2142-2154.

POWER, J. D., MITRA, A., LAUMANN, T. O., SNYDER, A. Z., SCHLAGGAR, B. L. & PETERSEN, S. E. 2014. Methods to detect, characterize, and remove motion artifact in resting state fMRI. *Neuroimage,* 84, 320-341.

PROSKOVEC, A. L., HEINRICHS-GRAHAM, E., WIESMAN, A. I., MCDERMOTT, T. J. & WILSON, T. W. 2018. Oscillatory dynamics in the dorsal and ventral attention networks during the reorienting of attention. *Human brain mapping,* 39, 2177-2190.

RAWJI, V., LATORRE, A., SHARMA, N., ROTHWELL, J. C. & ROCCHI, L. 2020. On the use of TMS to investigate the pathophysiology of neurodegenerative diseases. *Frontiers in neurology,* 11, 584664.

RUSHWORTH, M. F., ELLISON, A. & WALSH, V. 2001. Complementary localization and lateralization of orienting and motor attention. *Nature neuroscience,* 4**,** 656-661.

SATURNINO, G. B., MADSEN, K. H. & THIELSCHER, A. 2019. Electric field simulations for transcranial brain stimulation using FEM: an efficient implementation and error analysis. *Journal of neural engineering,* 16**,** 066032.

SCHUWERK, T., SCHURZ, M., MÜLLER, F., RUPPRECHT, R. & SOMMER, M. 2017. The rTPJ's overarching cognitive function in networks for attention and theory of mind. *Social cognitive and affective neuroscience,* 12**,** 157-168.

SEGAL, E. & PETRIDES, M. 2012. The morphology and variability of the caudal rami of the superior temporal sulcus. *European Journal of Neuroscience,* 36**,** 2035-2053.

SHULMAN, G. L., ASTAFIEV, S. V., FRANKE, D., POPE, D. L., SNYDER, A. Z., MCAVOY, M. P. & CORBETTA, M. 2009. Interaction of stimulus-driven reorienting and expectation in ventral and dorsal frontoparietal and basal ganglia-cortical networks. *Journal of Neuroscience,* 29**,** 4392-4407.

SMALL, D. M., GITELMAN, D. R., GREGORY, M. D., NOBRE, A. C., PARRISH, T. B. & MESULAM, M.-M. 2003. The posterior cingulate and medial prefrontal cortex mediate the anticipatory allocation of spatial attention. *Neuroimage,* 18**,** 633-641.

SZCZEPANSKI, S. M., PINSK, M. A., DOUGLAS, M. M., KASTNER, S. & SAALMANN, Y. B. 2013. Functional and structural architecture of the human dorsal frontoparietal attention network. *Proceedings of the National Academy of Sciences,* 110**,** 15806-15811.

THIEL, C. M., ZILLES, K. & FINK, G. R. 2004. Cerebral correlates of alerting, orienting and reorienting of visuospatial attention: an event-related fMRI study. *Neuroimage,* 21**,** 318-328.

THIELSCHER, A., ANTUNES, A. & SATURNINO, G. B. Field modeling for transcranial magnetic stimulation: A useful tool to understand the physiological effects of TMS? 2015 37th annual international conference of the IEEE engineering in medicine and biology society (EMBC), 2015. IEEE, 222-225.

TUSTISON, N. J., AVANTS, B. B., COOK, P. A., ZHENG, Y., EGAN, A., YUSHKEVICH, P. A. & GEE, J. C. 2010. N4ITK: improved N3 bias correction. *IEEE transactions on medical imaging,* 29**,** 1310-1320.

VAN HOORNWEDER, S., MEESEN, R. & CAULFIELD, K. A. 2022. On the importance of using both T1-weighted and T2-weighted structural magnetic resonance imaging scans to model electric fields induced by non-invasive brain stimulation in SimNIBS. *Brain Stimulation,* 15**,** 641-644.

VOSSEL, S., GENG, J. J. & FINK, G. R. 2014. Dorsal and ventral attention systems: distinct neural circuits but collaborative roles. *The Neuroscientist,* 20**,** 150-159.

WAGNER, T., GANGITANO, M., ROMERO, R., THÉORET, H., KOBAYASHI, M., ANSCHEL, D., IVES, J., CUFFIN, N., SCHOMER, D. & PASCUAL-LEONE, A. 2004. Intracranial measurement of current densities induced by transcranial magnetic stimulation in the human brain. *Neuroscience letters,* 354**,** 91-94.

WALSH, V. & COWEY, A. 2000. Transcranial magnetic stimulation and cognitive neuroscience. *Nature Reviews Neuroscience,* 1**,** 73-80.

WANG, J., ZHANG, J., RONG, M., WEI, X., ZHENG, D., FOX, P. T., EICKHOFF, S. B. & JIANG, T. 2016. Functional topography of the right inferior parietal lobule structured by anatomical connectivity profiles. *Human brain mapping,* 37**,** 4316-4332.

WEISE, K., NUMSSEN, O., KALLOCH, B., ZIER, A. L., THIELSCHER, A., HARTWIGSEN, G. & KNÖSCHE, T. R. 2022. Localization of cortical TMS effects and accurate motor threshold determination. *Nature protocols*.

WEISE, K., NUMSSEN, O., THIELSCHER, A., HARTWIGSEN, G. & KNÖSCHE, T. R. 2020. A novel approach to localize cortical TMS effects. *Neuroimage,* 209**,** 116486.

WILLIAMS, K. A., NUMSSEN, O. & HARTWIGSEN, G. 2022. Task-specific network interactions across key cognitive domains. *Cerebral Cortex,* 32**,** 5050-5071.

ZHANG, Y., BRADY, M. & SMITH, S. 2001. Segmentation of brain MR images through a hidden Markov random field model and the expectation-maximization algorithm. *IEEE transactions on medical imaging,* 20**,** 45-57.